Published in final edited form as:
Nat Struct Mol Biol. 2010 September ; 17(9): 1058–1064. doi:10.1038/nsmb.1883.

Molecular basis of FIR-mediated *c-myc* transcriptional control

Cyprian D. Cukier[1], **David Hollingworth**[1], **Stephen R. Martin**[2], **Geoff Kelly**[3], **Irene Díaz-Moreno**[1,4], and **Andres Ramos**[1]

[1]Molecular Structure Division, MRC National Institute for Medical Research, The Ridgeway, Mill Hill, London NW7 1AA, UK

[2]Physical Biochemistry Division, MRC National Institute for Medical Research, The Ridgeway, Mill Hill, London NW7 1AA, UK

[3]MRC Biomedical NMR Centre, The Ridgeway, Mill Hill, London NW7 1AA, UK

[4]Instituto de Bioquimica Vegetal y Fotosintesis, US-CSIC, Avda. Amerigo Vespucio 49, 41092, Sevilla, Spain

Abstract

The Far UpStream Element (FUSE) regulatory system promotes a peak in the concentration of c-Myc during cell cycle. First, the FBP transcriptional activator binds to the FUSE DNA element upstream of the *c-myc* promoter. Then, FBP recruits its specific repressor (FIR) which acts as an on/off transcriptional switch. Here we describe the molecular basis of FIR recruitment showing that the tandem RNA recognitions motifs of FIR provide a platform for independent FUSE DNA and FBP protein binding and explaining the structural basis of the reversibility of the FBP-FIR interaction. We also show that the physical coupling between FBP and FIR is modulated by a flexible linker positioned sequentially to the recruiting element. Our data explain how the FUSE system regulates precisely *c-myc* transcription and suggest that a small change in FBP–FIR affinity leads to a substantial effect on c-Myc concentration.

The *c-myc* proto-oncogene regulates the proliferation, growth and differentiation of somatic cells, integrating a number of intracellular and extracellular programs of gene control. c-Myc targets the PolII-dependent promoter of 10–15% of genes, including transcription factors, mRNA metabolism proteins, DNA repair factors, telomerases and cytokines [1,2]. Further, it modulates the transcription of a number of non-coding RNAs [3]. *c-myc* mis-regulation has been correlated with a broad range of cancer pathologies [4].

The Far Upstream Sequence Element (FUSE) upstream of the *c-myc* promoter mediates a fast transcription-responsive mechanism responsible for an upsurge of c-Myc levels during the cell cycle. FUSE-based c-Myc upregulation is mediated by the unwinding and opening of an AT-

Correspondence should be addressed to A.R. (aramos@nimr.mrc.ac.uk).

Author contributions

Cloning was performed by D.H. and C.C. Expression and purification of the FBP and FIR constructs were performed by C.C. and D.H. NMR spectra were recorded by C.C. and G.K. and analyzed by C.C. The structures in this paper were calculated by C.C. All NMR titrations were performed by C.C. SIA analysis was performed by I.D.M. CD data were recorded by A.R. and analyzed by S.M. BLI data were recorded and analyzed by C.C. and S.M. The paper was written by C.C. and A.R. All authors were involved in planning the experiments.

Accession Codes: Protein Data Bank: Coordinates of the structure of FIR RRM1-RRM2 alone and in complex with FBP Nbox have been deposited with accession codes 2kxf and 2kxh respectively.

Supplementary Information accompanies the paper on www.nature.com/nature.

rich stretch (the FUSE sequence) located about 1.7 kb upstream of the *c-myc* promoter as a consequence of the negative supercoiling that accumulates during pre-existing lower-level transcriptional activity [5,6] (Fig. 1a). The FUSE DNA non-coding strand (henceforth referred to as ssFUSE or ssFUSE DNA) recruits the FUSE-Binding Protein (FBP) that, in turn, interacts with Transcriptional Factor IIH (TFIIH) – a complex multi-component machine involved in transcriptional initiation and promoter escape – and increases the rate of productive *c-myc* transcription [7,8]. This increase in transcription leads to further negative supercoiling and to further opening of the FUSE. The FBP–FUSE complex recruits the FBP-Interacting Repressor (FIR) protein that interacts with both FBP and ssFUSE DNA. Upon binding to FBP and ssFUSE, FIR interacts with TFIIH [7] reducing FBP-mediated transcription and therefore negative supercoiling. FIR-mediated transcriptional repression leads to re-winding of the FUSE, ejection of FBP and, eventually, ejection of FIR itself, bringing the system back to a basal transcription state (Fig. 1a).

The FUSE regulatory system can be represented by a simple three-component mechanism to control *c-myc* transcription and is a promising tool in colorectal cancer therapy [9,10]. Central to FUSE regulation is the FIR–FBP interaction that mediates FIR recruitment and transcriptional shut-off. It has been shown that ssFUSE DNA binds to the tandem RNA Recognition Motifs (RRMs) of FIR (RRM1-RRM2) and to the four K-Homology (KH) domains of FBP (Fig. 1b) [11-13] but also that a direct FBP–FIR interaction takes place via a 26-aa element in the amino-terminus of FBP (called the Nbox, Fig. 1b) and the FIR RRM1-RRM2 tandem domains [11].

The importance of this interaction has been established by Chung and co-workers [11] who analyzed the activity of FIR in the FBP–DNA and FBP3–DNA transcriptional activation systems. FBP3 (Fig. 1b), a protein of the FBP family, has been shown to be expressed at different times than FBP during the cell cycle, and not to be affected by FIR-mediated repression [11,14]. Chung and co-workers have shown that FBP Nbox mediates an interaction between FBP and FIR while FBP3 Nbox lacks this capability. They have also shown that when the low efficiency of FIR recruitment to the DNA–FBP3 system is by-passed by fusing FIR to a high affinity DNA binding domain, FIR can repress FBP3. This indicates that Nbox-mediated recruitment of FIR to the DNA is a crucial step of control of FIR repressional activity [11].

Despite the availability of a broad range of functional information, our molecular understanding of FUSE mediated regulation – and therefore our capability to interfere with it – is severely limited by the lack of structural data on the FBP–FIR interaction and by the paucity of quantitative data on the protein–protein and protein–DNA interactions that build FUSE regulation. Here we focus on the molecular mechanism of FIR recruitment and on the FIR–FBP interaction that defines the length and intensity of *c-myc* upregulation during cell cycle. We use human (*Homo sapiens*) FIR and FBP proteins and FUSE DNA to explain why FBP is recruited before FIR in the FUSE functional cycle and how the necessary combination of specificity and reversibility is achieved by the Nbox–FIR interaction. Further, we quantify directly the effect of the Nbox in a model FBP–FIR–FUSE system and the decoupling effect of an unfolded linker located between the Nbox and the DNA-binding region of FBP. We conclude that the switch of the FUSE system from an activating to a repressing state is based on a relatively modest increase in the affinity of FIR for the FBP–FUSE DNA complex.

Results

Structure, dynamics and DNA binding properties of FIR RRM1-RRM2

To understand the molecular basis of FIR recruitment we need to characterize the structure of the FIR RRM1-RRM2 tandem domains and their interactions with FBP and with FUSE DNA. We have solved the solution structure of FIR RRM1-RRM2 alone and in complex with the FBP Nbox and showed that in FIR RRM1-RRM2 the helical face of RRM1 packs onto the β-

sheet face of RRM2, creating a stable interface (1,100 Å^2 of buried surface) (Figure 2a, Supplementary Fig. 1 and Table 1). This orientation is similar to what is observed in the structure of the DNA-bound FIR RRM1-RRM2 [15] (Supplementary Fig. 1b). NMR relaxation data confirm that binding of FIR to the FBP and FUSE binding partners does not lead to conformational rearrangements in the protein (Supplementary Fig. 2).

The arrangement of RRM1 and RRM2 described above indicates that only the β-sheet nucleic acid binding surface of RRM1 is available for DNA binding. Our NMR Chemical Shift Perturbation (CSP) data confirm that DNA binding involves canonical nucleic acid binding RiboNucleoProtein (RNP2 and RNP1) motifs plus residues in the α2/β4, β1/α1 and β2/β3 loops of RRM1, including the residues making contact with the single nucleotide visible in the published structure of the DNA-bound FIR RRM1-RRM2 [15] (Fig. 2b). Based on the known RRM–nucleic acid structures, this surface is likely to accommodate a 4–5 nucleotides long DNA sequence [16] and therefore we have explored the nucleobase preference of FIR for four successive nucleotides positions using Scaffold Independent Analysis (SIA) [17]. We show that FIR RRM1-RRM2 has a moderate sequence preference for T or T/G in all of the four positions analyzed by SIA (Fig. 2c, Supplementary Table 1). We use follow-up NMR binding assays with DNA 5-mers of different base compositions to confirm this sequence preference and to define a range of affinities for FIR interaction with optimal and non-optimal DNA sequences (Fig. 2c). Knowing FIR's sequence preference and the range of affinities for different DNA sequences allows a more accurate understanding of FIR–FUSE interactions.

FIR–FUSE and FBP–FUSE interactions

In order to define accurate models for FBP and FIR recruitment and ejection it is necessary to quantify the strength of the FIR–FUSE interaction and to compare it with the FBP–FUSE interaction. A preliminary model for FBP recruitment put forward by Liu and co-workers predicts that ssFUSE has a higher affinity for FIR than for FBP and proposes that the initial recruitment of FBP – rather than FIR – to the ssFUSE is due to the higher concentration of FBP in the cell [8] while a recent paper published during revision of our work indicates that the affinity of FIR for the FUSE is the same or lower by a factor of 5 than the one of FBP, depending on the FUSE DNA used [18]. Considering that FIR and FBP can bind to overlapping sequences in the FUSE [12] a similar affinity of the two proteins for the DNA would indicates that the choice of recruiting FBP rather than FIR is dependent on the variations of their concentration in the cell. To clarify if the earlier binding of FBP to the FUSE is dependent on the concentration of FBP and FIR, we have recorded BioLayer Interferometry (BLI) experiments using an immobilized 40-mer ssFUSE (ssFUSE40, Fig. 1a) and increasing concentrations of FIR (Fig. 2d). This DNA has been designed to recapitulate the areas of interactions of FIR and FBP as defined by Benjamin *et al.* [12] . We show that FIR binds to the FUSE with a K_d value of ~7 μM, as determined from the ratio of the dissociation and association rate constants, and independently from analysis of the dependence of the amplitude of the BLI signal on FIR concentration. Instead, BLI experiments report that the complexes between ssFUSE40 DNA and two FBP KH domains constructs with and without the Nbox (Fig. 1b) have dissociation constants in the ~1.5–2 nM range (Fig. 2d, Supplementary Fig. 3, Supplementary Table 2). So, FBP–ssFUSE binding is three orders of magnitude stronger than FIR–ssFUSE binding and therefore the initial recruitment of FBP in the cell is driven by its higher affinity for the ssFUSE. The association of FBP with the DNA is long lasting (k_{off} ~4×10^{-4} s^{-1}, Supplementary Fig. 3), consistent with the prolonged TFIIH-mediated enhancement of productive *c-myc* transcription observed upon eliminating FIR downregulation of TFIIH [8].

FIR dimerization on the FUSE has been proposed to lead to FBP ejection [15] or to guide rearrangement of the FUSE–FBP–FIR complex [18]. FIR was proposed to form a dimer while bound to ssDNA based on the X-ray structure of that complex (where the protein crystallizes

as a dimer in the asymmetric unit, Fig. 3a) and on the 2:1 stoichiometry obtained from Size Exclusion Chromatography coupled with Light Scattering, Refractive Index and UltraViolet absorbance (SEC-LS/RI/UV) data. We used NMR to investigate this possibility. Our assays show that two molecules of FIR bind to a single ssFUSE-derived 29-mer used in functional studies [11] (ssFUSE29, Fig. 1a) and that the affinity for the two equivalent or quasi-equivalent protein binding sites is in the low micromolar range (Fig. 3b), consistent with the BLI data and with the fast exchange regime of the shifting resonances. This is consistent with the 2:1 stoichiometry that has been reported for a similar FIR–FUSE DNA complex [15]. However, our data also show that FIR does not dimerize upon binding the FUSE (ssFUSE29). We analyzed the chemical shifts of all of the amide protons within 10 Å of the protein–protein inter-molecular interface, as derived from the X-ray structure (Fig. 3a). In RRM2, which is important to dimerization and is far away from the actual DNA-binding surface, none of the well dispersed protons frequencies of the monomeric free RRM1-RRM2 is affected upon ssFUSE29 binding, suggesting that the dimer is not formed. In RRM1 the proposed dimer interface is in close proximity to the DNA binding surface and some chemical shift changes from DNA binding are likely to affect residues in the putative dimer interface. To decouple dimerization from DNA binding, we compared the CSP recorded upon RRM1–ssFUSE29 binding to the ones recorded upon RRM1 interaction with the DNA pentamers described in the previous paragraph – that bind with a 1:1 FIR:DNA stoichiometry. Very similar chemical shift changes are obtained for the two DNA molecules indicating that RRM1 is not involved in dimerization either (Fig. 3c, Supplementary Results). Further, NMR relaxation data show that the rotational correlation time of the DNA-bound protein is lower than the one expected if the two proteins would make contact forming a compact 50 kDa complex (Supplementary Fig. 2a, Supplementary Results). The binding of more than one FIR molecule on the FUSE is consistent with the relaxed T/TG sequence preference of FIR, as described above but the chemical shift changes we observe upon FIR–DNA interactions show unambiguously that dimerization does not take place. It is unclear whether the binding of more than one FIR on the free FUSE DNA that we observe has any physiological relevance, as in the cell FBP binds before FIR reducing the ssDNA available for FIR binding and one copy only of FIR can be recruited by the FBP Nbox.

FIR–FBP interaction

We then examined the interaction between FIR RRM1-RRM2 and the FBP Nbox that is essential for FIR recruitment to FUSE DNA [11]. Our NMR data reveal that the FBP Nbox assumes a helical conformation and docks on a hydrophobic surface defined by α1, α2 and the β1/α1 and α2/β4 loops (Fig. 4 and Supplementary Fig. 4 and 5) of the RRM2 domain of FIR (K_d ~15 μM, Fig. 4a and Supplementary Table 2). The binding of a helical element in an orientation quasi-parallel to RRM1 α1 has never been observed before in protein–RRM interactions and the FBP–FIR structure presented here defines a novel protein interaction surface on the multi-functional RRM platform (Fig. 5) [16]. The peptide–protein contacts are mostly hydrophobic (Fig. 4d and Supplementary Fig. 4b) and an overview of the interface shows that two alanine residues from the Nbox (Ala34 and Ala38) occupy the central part of the peptide recognition surface and are flanked by bulkier hydrophobic residues (e.g. Phe31, Leu35, Ile41) (Fig. 4c and Supplementary Fig. 4b). This arrangement results in a very limited inter-digitation between side chains of FBP and FIR residues and in low frequency motions at the FBP–FIR interface (Supplementary Fig. 2 and Supplementary Results). The position of these two alanine residues explains the results of a recent mutational study [11] in which a very strong binding impairment was observed for A34V and A38V mutants. The mutations place a large hydrophobic chain in the center of the inter-molecular interface, resulting in steric hindrance (Supplementary Fig. 4b). In the same study, Chung and co-workers showed that mutation of Leu35 or Phe31 to alanine has a substantial but smaller effect, which can be explained by the loss of the specific interactions mediated by their two partially packed side chains (Fig. 4c and Supplementary Fig. 4b). By contrast, mutation of Ala42 (A42V) – that we

show to be very loosely packed against the RRM2 surface (Supplementary Fig. 4b) – does not lead to substantial loss of binding. Our structure reveals that the side chains arrangement on the FBP–FIR interaction surface is designed to provide a low affinity but specific recognition. The dramatic loss of binding obtained by inserting a bulky hydrophobic side chain in the solvent-excluded part of the interface indicates that the helix, although in a dynamic interaction, cannot re-orient freely on the RRM2 surface. It seems likely that the global specificity is provided by the sum of the hydrophobic contacts made by the different side chains of the hydrophobic face of the Nbox helix. Indeed when Chung and co-workers mutate simultaneously both Leu35 and Phe31 to alanine the loss of binding is stronger that the one observed for the single mutants. Relaxation data on the bound RRM1-RRM2 and the broadening of several peptide resonances at the protein–peptide interface (Supplementary Methods, Supplementary Fig. 2) are consistent with the structural information on the complex and with the transient nature of the FIR–FBP contacts in the FUSE-mediated *c-myc* regulation – in which the ejection of FBP precedes FIR ejection and is dependent on the disruption of the FBP–FIR interaction (Fig. 1a).

The FBP–FIR–FUSE system

What is the relationship between protein binding and DNA binding on the FIR RRM1-RRM2? DNA and protein interaction surfaces are on different domains and on opposite sides of the RRM1-RRM2 protein (Fig. 6a). The chemical shift changes induced by the two binding partners are additive (Fig. 6b), indicating that the two binding events are independent. Indeed, the affinity of RRM1-RRM2 for the short TGTGT DNA oligo does not change when the FBP Nbox peptide is also bound and *vice versa* (Supplementary Fig. 6, Supplementary Table 2). This confirms that no allosteric cooperativity is present between Nbox and ssFUSE DNA binding. Therefore the reported effect of the Nbox on FIR recruitment is due to the physical tethering that exists between FBP and FIR in the larger three-component FBP–FIR–ssFUSE system. The lack of an allosteric effect in RRM1-RRM2 is consistent with the lack of conformational changes upon binding the FBP Nbox peptide and the ssFUSE DNA (Supplementary Fig. 1b).

The effect of physical tethering by FBP on FIR DNA binding activity was directly measured using BLI and a larger FBP–FIR–DNA three-component system (Fig. 7a). 150 nM FIR RRM1-RRM2 does not show detectable binding to the free DNA or to the DNA bound by the four KH domain FBP construct, while the addition of the Nbox recruiting element to the FBP construct stimulates the interaction (Fig. 7a). The K_d of FIR in the three-molecule complex, as estimated from the association and dissociation rate constants, is lower by a factor of 10–50 than the K_d of FIR for the free DNA (7 μM). This increase in affinity is modest, much lower than the one expected if the Nbox was structurally coupled to the first of the DNA binding modules (KH1) of FBP. The partial decoupling between DNA binding by FBP and FIR is explained by the presence of a ~50-amino acid unstructured linker that separates the Nbox from KH1 (Fig. 1b). The decoupling effect estimated for the FUSE system (by a factor of ~5,000) is consistent with the one calculated based on a model commonly used for two interacting regions separated by a flexible linker [19,20]. Such a decoupling effect has been often reported for RNA recognition by multi-domain proteins [21].

In order to validate the model above we provide direct experimental evidence that FIR RRM1-RRM2 and FBP Nbox do not interact with the KH region of FBP and that the Nbox-FIR RRM1-RRM2 unit is structurally decoupled from the DNA binding region of FBP. We have titrated an unlabeled sample of the FBP construct comprising both the Nbox and the KH domains into a ^{15}N labeled sample of FIR RRM1-RRM2 and recorded fingerprint NMR ^{15}N-^{1}H correlation NMR spectra. We have compared these spectra with the ones recorded during an equivalent titration performed using an unlabeled sample of the Nbox-only construct. The same pattern

of chemical shift changes is observed in both titrations (Supplementary Fig. 7a). This indicates that the Nbox–FIR interaction does not change whether the KH domains are present or not in the FBP construct and that neither the KH domains nor the linker interact with RRM1-RRM2. Further, the moderate increase in the line-width of the RRM1-RRM2 resonances (Supplementary Fig. 7b) provides independent evidence that the flexible linker between the Nbox and the KH domains structurally decouples FIR RRM1-RRM2 from the FBP KH domain region – if that was not the case a very severe broadening would be observed upon binding to the ~45 kDa FBP construct. Next, we have added FUSE DNA to the FIR RRM1-RRM2–FBP Nbox KH1-KH4 complex described above and recorded again a fingerprint NMR ^{15}N-^{1}H correlation NMR spectrum. A dramatic broadening is observed for FIR RRM1-RRM2 resonances upon addition of DNA. The broadening is more severe for resonances in the more rigid parts of the molecules (e.g. in the β-sheet) and is absent for resonances of the flexible C-terminus (Supplementary Fig. 7c). This indicates that both FBP and FIR bind at the same time to the FUSE DNA. Simultaneous binding establishes a second DNA-mediated physical link between FBP and FIR – strongly impairing the capability of the two molecules to tumble independently.

FBP3 interactions with FUSE and FIR

In order to investigate whether a 10–50 fold difference in affinity can justify recruitment of FIR in a cellular environment, we compared protein–protein and protein–DNA interactions in the FBP and FBP3 systems. Using BLI we show that a FBP3 Nbox-KH1-KH4 construct binds to the FUSE element (ssFUSE40) with an affinity comparable to the one of FBP (K_d = 1.1 nM) (data not shown, Supplementary Table 2). However, when we added FIR to the FBP3 Nbox-KH1-KH4–FUSE system no Nbox-dependent binding of FIR to the DNA was observed (Fig. 7b). This is consistent with the published data that indicate that FBP3 Nbox does not recruit FIR in the cell, and confirms that the Nbox-dependent recruitment of FIR we observe by BLI mirrors the functionally relevant recruitment of FIR. Next, we established the difference in affinity of FBP and FBP3 Nboxes for FIR RRM1-RRM2 that leads to the loss of functional recruitment. We measured the affinity of the FBP3 Nbox–FIR RRM1-RRM2 interaction: the K_d of the complex is 280 ± 36 μM and is higher than the one of the FBP Nbox–FIR RRM1-RRM2 complex by a factor of ~20 (Fig. 7c). That is, a drop by a factor of ~20 in affinity corresponds to a loss of function in the FBP(s) Nbox–FIR interaction.

Discussion

The work presented here explains the molecular basis of FIR-mediated *c-myc* regulation. We show that the initial recruitment of FBP by the partially open FUSE is justified by its high affinity for a specific site on the DNA. FIR is then recruited by concurrent FBP and DNA binding, and separate FIR–FBP and FIR–DNA interactions are established on FIR RRM1-RRM2. It has been shown that a single RRM domain (RRM2 of Raver1) can bind simultaneously to protein and RNA targets [22,23]. The use of two RRM domains in FIR is therefore not an absolute requirement imposed by the small size of the RRM domain but a characteristic of this specific system. In FIR, the physical separation of the DNA and FBP binding surfaces (Fig. 6a) minimizes interference between binding events in the three-subunit complex. This separation is functionally important, because the FBP–FIR interaction must be disrupted upon FBP ejection while FIR remains bound to the DNA. The use of a central patch of alanines surrounded by larger hydrophobic residues to create a transient and yet specific interaction is, as far as we are aware of, described here for the first time. It will be of interest to explore whether such a pattern defines other transient protein–protein interactions.

Assembly of the FIR-containing complex (and therefore transcriptional repression) is controled by the relatively low affinity, high specificity FBP–FIR interaction [11], which is based on a

novel, non-canonical mode of RRM–protein recognition. The sequence of FBP and FIR dissociation in the cell must be, at least partially, controled by other protein–protein interactions. The binding affinity we measure for the FIR–FUSE interaction (K_d ~7 μM) is altogether not sufficient to maintain the observed FIR–DNA binding after FBP has dissociated [8].

The FUSE mechanism is based on a single activator (FBP) recruiting its own (single) repressor (FIR). This allows the establishment of a functional relationship between the length of the activation step and the weak coupling between FBP and FIR binding to ssFUSE. A strong cooperativity of FBP–FIR binding on the DNA would speed FIR recruitment beyond what is desirable and would reduce the peak of *c-myc* expression (Fig. 7d). Instead, the long flexible linker and the weak Nbox–FIR interaction create a weak coupling between the two proteins that can be regulated more subtly. Interestingly, the analysis of the interaction between FBP3 Nbox and FIR shows that a drop by a factor of 20 in the strength of the interaction impairs functional FIR recruitment in the cell, confirming a regulatory model where a change in affinity of one–two orders of magnitude regulates an important transcriptional switch. Recent work has asserted the potential of targeting *c-myc* as an anticancer strategy [24] suggesting that *c-myc* repression could be explored as a therapeutic strategy. Our work reveals how the modulation of FBP–FIR coupling allows an initial period of unhindered FBP-promoted transcription. This opens the exciting possibility that compounds that stabilize the Nbox–RRM2 interaction could speed FIR recruitment and reduce productive transcription of *c-myc* (Fig. 7d).

Methods

Protein preparation

FIR RRM1-RRM2 (amino-acids 103–297, NP_055096) were cloned into pETM-30 vector (EMBL-Heidelberg, Protein Expression Facility), introducing TEV protease-cleavable HisTag-GST fusion N-terminal to the insert. The HisTag-GST fusion protein was purified from the soluble fraction by nickel-affinity chromatography (Qiagen) followed by gel filtration. The final protein was concentrated to 0.4–0.6 mM and stored in 10 mM Tris-HCl pH 8.0 (or 7.4), 50 mM NaCl, 2 mM Tris(2-carboxyethyl)phosphine (TCEP), 0.05% (w/v) NaN_3 in the presence of protease inhibitors (Roche) at −80 °C.

Unlabeled FBP Nbox peptide (amino-acids 27–52, NP_003893) with and without an N-terminal Y residue and unlabeled FBP3 Nbox (amino-acids 15–40, NP_003925) were chemically synthesized (Peptide Synthesis Facility, University of Bristol and in-house, respectively). The addition of Y residue does not affect FBP Nbox–FIR RRM1-RRM2 interaction as assessed by NMR titrations (data not shown). Labeled (^{15}N or $^{15}N^{13}C$) FBP Nbox peptide (with N-terminal Y) was cloned and expressed as described for FIR RRM1-RRM2 and then purified from the soluble fraction by nickel-affinity chromatography (Qiagen) followed by HPLC purification. The peptide was stored in 10 mM Tris-HCl pH 5.0 (or 8.0), 0.05% (w/v) NaN_3 in the presence of protease inhibitors (Roche) at −80 °C.

FBP Nbox-KH1-KH4 (amino-acids 27–455, NP_003893), FBP KH1-KH4 (amino-acids 85–455, NP_003893) and FBP3 Nbox-KH1-KH4 (amino-acids 13–431, NP_003925) were cloned, expressed and purified by nickel-affinity chromatography as described for FIR RRM1-RRM2. The protein was further purified on anion exchange and heparin affinity columns. The proteins were stored in 10 mM Tris-HCl pH 7.4, 50 mM NaCl, 2 mM TCEP, 0.05% (w/v) NaN_3 in the presence of protease inhibitors (Roche) at −80 °C.

For details of the protein preparations see the online Supplementary Methods section.

ssDNA oligonucleotides

All ssDNA oligonucleotides and SIA oligonucleotides pools were chemically synthesized (Sigma and Integrated DNA Technologies). ssFUSE40 corresponds to nucleotides 769–808 in the complementary strand to X00364 entry.

NMR spectroscopy

All NMR experiments were recorded at 37 °C or 45 °C on Varian Inova and Bruker Avance spectrometers equipped with cryoprobes and operating at 600, 700 and 800 MHz ^{1}H frequencies. The spectra were processed with the NMRPipe package [27] and analyzed with Sparky [28]. Further details can be found in Supplementary Methods.

Structure calculations

Distance and angle restraints were used to perform structure calculations with ARIA 1.2 [29]. Experimental distance restraints were achieved by integrating Sparky assigned NOE peaks with XEASY [30]. Dihedral restraints (φ and ψ) were obtained from the chemical-shift-based TALOS database [31]. For the free and bound proteins, H-bond restraints were added in subsequent calculations if an exchange-protected $^{1}H^{N}$ was H-bonded in at least 50% of the preliminary structures generated in a given run. For the peptide, the H-bond restraints of a standard α-helix were added in the helical region (Ala30–Lys44).

In iterations 0–7 of ARIA calculations fifty randomized conformers were subject to simulated annealing with a standard CNS protocol [32]. The ten lowest-global-energy structures were used for assignment at the next iteration. In iteration 8 the number of generated structures was increased to 200. Finally, the 20 lowest-energy obtained structures were water refined [33]. The quality of each generated family was evaluated with PROCHECK_NMR [34]. Ramachandran plot statistics for FIR RRM1-RRM2: Most favored regions 83.9%, Additional allowed regions 14.3%, Generously allowed regions 0.9%, Disallowed regions 0.9%. Ramachandran plot statistics for FIR RRM1-RRM2–FBP Nbox complex: Most favored regions 82.2%, Additional allowed regions 15.3%, Generously allowed regions 1.0%, Disallowed regions 1.5%. The structures were displayed and analyzed with MOLMOL [26], PYMOL (www.pymol.org) and InsightII (Accelrys).

Circular Dichroism (CD)

Far-UV CD spectrum of 50 μM FBP Nbox in 10 mM Tris-HCl pH 7.4, 20 mM NaCl was recorded at 5 °C on a Jasco J-715 spectropolarimeter (Jasco) equipped with a PTC-348 Peltier temperature-control system. The CD signal is reported as the mean residue CD extinction coefficient ($\Delta\varepsilon_{MRW}$).

Binding assays: NMR

NMR titrations were performed by titrating unlabeled interacting partner into solution of ^{15}N-labeled sample (for details see Supplementary Methods). ^{15}N sofast HMQC spectra [35] were recorded at each titration point at 37 °C or 45 °C on Varian Inova and Bruker Avance spectrometers equipped with cryoprobes and operating at 600, 700 and 800 MHz ^{1}H frequencies. To obtain K_d values the average chemical shift perturbations ($\Delta\delta_{avg} = ((\Delta\delta_N/10)^2 + \Delta\delta_H^2)^{1/2}$) of 7–10 peaks were plotted as a function of ligand:protein ratio, followed by two-parameter nonlinear least-squares fit of the data for each peak in the program Origin (OriginLab), using a one-site binding model which corrects for dilution effect [36]. K_d values are reported as average ± 2 standard deviations.

Binding assays: SIA

SIA analysis was performed as described in Beuth *et al.* [17] with 16 pools of 5-mer DNA oligonucleotides (nANNN, nGNNN, nCNNN etc.). In brief, solutions of 25 μM ^{15}N-labeled FIR RRM1-RRM2 in 10 mM Tris-HCl pH 7.4, 50 mM NaCl, 2 mM TCEP were titrated with individual DNA pools (ratios 1:0, 1:1 and 1:4). ^{15}N sofast HMQC spectra [35] were recorded at each titration point at 37 °C on a Varian Inova spectrometer equipped with cryoprobe and operating at 800 MHz ^{1}H frequency. Average chemical shift perturbations ($\Delta\delta_{avg} = ((\Delta\delta_N/10)^2 + \Delta\delta_H^2)^{1/2}$) of 15 peaks were analyzed to obtain SIA scores. The results were visualized with WebLogo (http://weblogo.berkeley.edu/logo.cgi).

Binding assays: BLI

All BLI experiments were performed in 10 mM Tris-HCl pH 7.4, 150 mM NaCl, 2 mM TCEP, 0.5 mg ml^{-1} BSA on an Octet Red instrument (ForteBio, Inc., Menlo Park, CA) operating at 25 °C. Streptavidin coated biosensors with immobilized biotinylated ssFUSE40 (Sigma) were exposed to different concentrations of FIR RRM1-RRM2, FBP Nbox-KH1-KH4, FBP KH1-KH4 or FBP3 Nbox-KH1-KH4 or combination of them as described in the Supplementary Results section.

Supplementary Material

Refer to Web version on PubMed Central for supplementary material.

Acknowledgments

We would like to thank Drs A. Oreggioni and T. Frenkiel for help in recording NMR experiments, Drs C. deChiara and G. Nicastro for advice on the ARIA protocols used in structure calculations, Dr. A. M. Candel for help with spectroscopic data and S. Kralovicova for general support in the lab. We would also like to thank Dr Peter Rosenthal for useful discussions. All NMR spectra were recorded at the MRC Biomedical NMR Centre. We would like to thank Dr S. Kindler (University of Hamburg) for the gift of a plasmid with the FIR RRM1-RRM2 gene. This work has been funded by the MRC Grant-in-aid U117574558.

References

1. Levens D. Disentangling the MYC web. Proc Natl Acad Sci U S A 2002;99:5757–5759. [PubMed: 11983876]
2. Wierstra I, Alves J. The *c-myc* promoter: still MysterY and challenge. Adv Cancer Res 2008;99:113–333. [PubMed: 18037408]
3. Kenneth NS, White RJ. Regulation by c-Myc of ncRNA expression. Curr Opin Genet Dev 2009;19:38–43. [PubMed: 19179065]
4. Meyer N, Penn LZ. Reflecting on 25 years with MYC. Nat Rev Cancer 2008;8:976–990. [PubMed: 19029958]
5. Kouzine F, Liu J, Sanford S, Chung HJ, Levens D. The dynamic response of upstream DNA to transcription-generated torsional stress. Nat Struct Mol Biol 2004;11:1092–1100. [PubMed: 15502847]
6. Kouzine F, Sanford S, Elisha-Feil Z, Levens D. The functional response of upstream DNA to dynamic supercoiling in vivo. Nat Struct Mol Biol 2008;15:146–154. [PubMed: 18193062]
7. Liu J, et al. Defective interplay of activators and repressors with TFIIH in xeroderma pigmentosum. Cell 2001;104:353–363. [PubMed: 11239393]
8. Liu J, et al. The FUSE/FBP/FIR/TFIIH system is a molecular machine programming a pulse of *c-myc* expression. EMBO J 2006;25:2119–2130. [PubMed: 16628215]
9. Matsushita K, et al. An essential role of alternative splicing of *c-myc* suppressor FUSE-binding protein-interacting repressor in carcinogenesis. Cancer Res 2006;66:1409–1417. [PubMed: 16452196]
10. Matsushita K, et al. *c-myc* suppressor FBP-interacting repressor for cancer diagnosis and therapy. Front Biosci 2009;14:3401–3408. [PubMed: 19273283]

11. Chung HJ, et al. FBPs are calibrated molecular tools to adjust gene expression. Mol Cell Biol 2006;26:6584–6597. [PubMed: 16914741]
12. Benjamin LR, et al. Hierarchical mechanisms build the DNA-binding specificity of FUSE binding protein. Proc Natl Acad Sci U S A 2008;105:18296–18301. [PubMed: 19015535]
13. Braddock DT, Louis JM, Baber JL, Levens D, Clore GM. Structure and dynamics of KH domains from FBP bound to single-stranded DNA. Nature 2002;415:1051–1056. [PubMed: 11875576]
14. Davis-Smyth T, Duncan RC, Zheng T, Michelotti G, Levens D. The far upstream element-binding proteins comprise an ancient family of single-strand DNA-binding transactivators. J Biol Chem 1996;271:31679–31687. [PubMed: 8940189]
15. Crichlow GV, et al. Dimerization of FIR upon FUSE DNA binding suggests a mechanism of *c-myc* inhibition. EMBO J 2008;27:277–289. [PubMed: 18059478]
16. Clery A, Blatter M, Allain FH. RNA recognition motifs: boring? Not quite. Curr Opin Struct Biol 2008;18:290–298. [PubMed: 18515081]
17. Beuth B, Garcia-Mayoral MF, Taylor IA, Ramos A. Scaffold-independent analysis of RNA-protein interactions: the Nova-1 KH3–RNA complex. J Am Chem Soc 2007;129:10205–10210. [PubMed: 17655233]
18. Hsiao HH, et al. Quantitative Characterization of the Interactions between *c-myc* Transcriptional Regulators FUSE, FBP and FIR. Biochemistry 2010;49:4620–4623. [PubMed: 20420426]
19. Shamoo Y, Abdul-Manan N, Williams KR. Multiple RNA binding domains (RBDs) just don't add up. Nucleic Acids Res 1995;23:725–728. [PubMed: 7535921]
20. Shamoo Y, et al. Both RNA-binding domains in heterogenous nuclear ribonucleoprotein A1 contribute toward single-stranded-RNA binding. Biochemistry 1994;33:8272–8281. [PubMed: 7518244]
21. Lunde BM, Moore C, Varani G. RNA-binding proteins: modular design for efficient function. Nat Rev Mol Cell Biol 2007;8:479–490. [PubMed: 17473849]
22. Rideau AP, et al. A peptide motif in Raver1 mediates splicing repression by interaction with the PTB RRM2 domain. Nat Struct Mol Biol 2006;13:839–848. [PubMed: 16936729]
23. Lee JH, Rangarajan ES, Yogesha SD, Izard T. Raver1 interactions with vinculin and RNA suggest a feed-forward pathway in directing mRNA to focal adhesions. Structure 2009;17:833–842. [PubMed: 19523901]
24. Soucek L, et al. Modelling Myc inhibition as a cancer therapy. Nature 2008;455:679–683. [PubMed: 18716624]
25. Corsini L, et al. Dimerization and protein binding specificity of the U2AF homology motif of the splicing factor Puf60. J Biol Chem 2009;284:630–639. [PubMed: 18974054]
26. Koradi R, Billeter M, Wuthrich K. MOLMOL: a program for display and analysis of macromolecular structures. J Mol Graph 1996;14:51–55. [PubMed: 8744573]
27. Delaglio F, et al. NMRPipe: a multidimensional spectral processing system based on UNIX pipes. J Biomol NMR 1995;6:277–293. [PubMed: 8520220]
28. Sparky (computer program). University of California; San Francisco: 2004.
29. Linge JP, O'Donoghue SI, Nilges M. Automated assignment of ambiguous nuclear overhauser effects with ARIA. Methods Enzymol 2001;339:71–90. [PubMed: 11462826]
30. Bartels C, Xia T.-h. Billeter M, Güntert P, Wüthrich K. The program XEASY for computer-supported NMR spectral analysis of biological macromolecules. J Biomol NMR 1995;6:1–10.
31. Cornilescu G, Delaglio F, Bax A. Protein backbone angle restraints from searching a database for chemical shift and sequence homology. J Biomol NMR 1999;13:289–302. [PubMed: 10212987]
32. Brunger AT, et al. Crystallography & NMR system: A new software suite for macromolecular structure determination. Acta Crystallogr D Biol Crystallogr 1998;54:905–921. [PubMed: 9757107]
33. Linge JP, Williams MA, Spronk CA, Bonvin AM, Nilges M. Refinement of protein structures in explicit solvent. Proteins 2003;50:496–506. [PubMed: 12557191]
34. Laskowski RA, Rullmannn JA, MacArthur MW, Kaptein R, Thornton JM. AQUA and PROCHECK-NMR: programs for checking the quality of protein structures solved by NMR. J Biomol NMR 1996;8:477–486. [PubMed: 9008363]

35. Schanda P, Kupce E, Brutscher B. SOFAST-HMQC experiments for recording two-dimensional heteronuclear correlation spectra of proteins within a few seconds. J Biomol NMR 2005;33:199–211. [PubMed: 16341750]

36. Kannt A, Young S, Bendall DS. The role of acidic residues of plastocyanin in its interaction with cytochrome f. Biochim Biophys Acta 1996;1277:115–126.

UKPMC Funders Group Author Manuscript

UKPMC Funders Group Author Manuscript

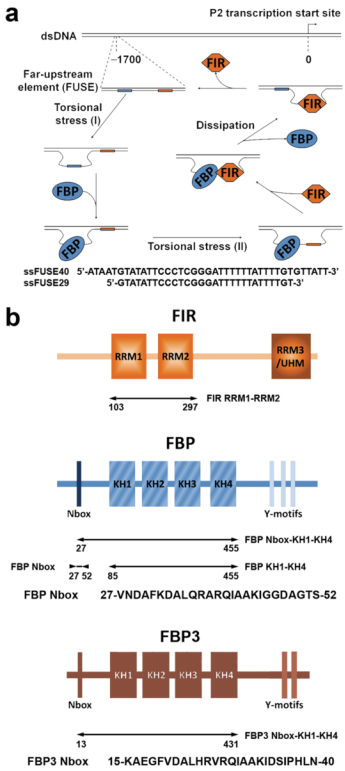

Figure 1.

FIR and FBP are nucleic acid binding proteins involved in *c-myc* transcription regulation. **(a)** Top – Model of FUSE-dependent regulation of *c-myc* proto-oncogene. Bottom – FUSE DNA sequences (non-coding strand) used in this study. **(b)** Domain organization of FIR, FBP and FBP3 with the protein constructs used in this study (indicated by arrows). Amino acid sequence of FBP and FBP3 Nbox are given.

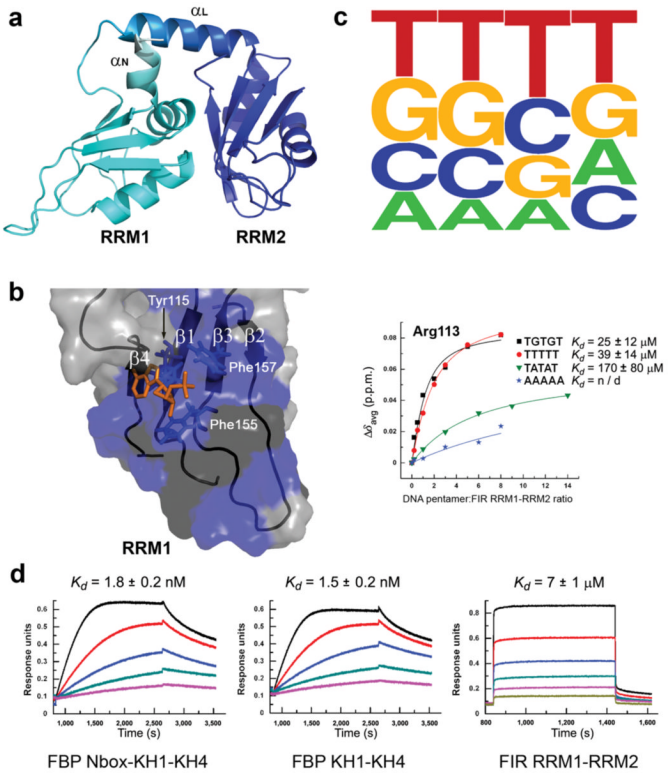

Figure 2.

FIR and FBP bind to ssFUSE DNA with different affinities. **(a)** Ribbon representation of FIR RRM1-RRM2. RRM1 is in light blue, RRM2 in dark blue and the amino terminal and linker alpha helices (α_N and α_L) are colored in white-to-light blue and a light blue-to-dark blue color gradients, respectively. **(b)** DNA binding surface of FIR RRM1. Residues showing substantial chemical shift perturbation (CSP) upon titration with the ssFUSE29 are in blue, residues whose amide resonance is not assigned are in dark grey. The position of the single nucleotide visible in the X-ray structure (orange) has been reported on the FIR RRM1-RRM2. The side chains of the aromatic residues located in the conserved RNP2 and RNP1 nucleic acids binding motifs (Tyr115, Phe155, Phe157) are displayed. The DNA molecule binds the canonical nucleic acid binding surface of the RRM1 domain. The structural representations in Figures 2a and 2b were generated using the program PYMOL (www.pymol.org). **(c)** Top – Graphic representation of FIR RRM1-RRM2 DNA sequence preference. The picture was generated by plotting our SIA data with the Weblogo server (http://weblogo.berkeley.edu/logo.cgi). Bottom – NMR binding isotherms of four ssDNA pentamers interacting with FIR RRM1-RRM2. The experiments were performed in 50 mM NaCl at 37 °C. RRM1-RRM2 has a moderate sequence specificity for Ts or Gs in all nucleobase positions. K_d are reported ± 2 × s.d. **(d)** Binding of increasing concentrations of FBP Nbox-KH1-KH4 (0.5 nM, 1 nM, 2 nM, 4 nM, 8 nM) (left), FBP KH1-KH4 (0.5 nM, 1 nM, 2 nM, 4 nM, 8 nM) (middle) and FIR RRM1-RRM2 (0.31 μM, 0.63 μM, 1.25 μM, 2.5 μM, 5 μM and 10 μM) (right) to ssFUSE40, as recorded by BLI. The experiments were performed in 150 mM NaCl at 25 °C. ssFUSE binding to FBP is three orders of magnitude tighter than FUSE binding to FIR. K_d are reported ± s.d.

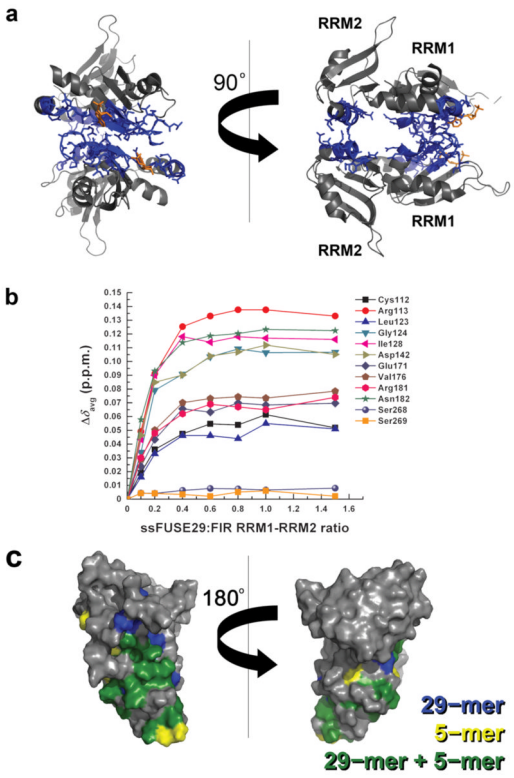

Figure 3.

DNA binding and protein dimerization by FIR RRM1-RRM2. **(a)** X-ray structure of FIR RRM1-RRM2 bound to ssFUSE DNA (2qfj). The FIR RRM1-RRM2 dimer is represented with a grey ribbon and residues whose H^N protons are less than 10 Å from the dimer interface are displayed in blue. The nucleotide visible in the X-ray structure is displayed in orange. This structural representation was generated using the program PYMOL (www.pymol.org). **(b)** Isotherms for binding of the ssFUSE29 DNA to FIR RRM1-RRM2 (NMR). Ser268 and Ser269 are two residues of RRM2 ~5 Å away from the proposed dimer interface which do not change their chemical shift in response to DNA binding. **(c)** CSP of FIR RRM1-RRM2 resonances upon addition of ssFUSE29 or TGTGT pentamer. CSP by the ssFUSE29 (blue) largely overlap with CSP by the TGTGT pentamer (yellow) defining a common binding surface (green). Small differences are observed in the protein N-terminal helix, that is opposite to the dimerization area which can be attributed to transient contact with additional nucleotides in the longer DNA. FIR RRM1-RRM2 does not dimerize on ssFUSE29 DNA. These structural representations were generated using the program PYMOL (www.pymol.org).

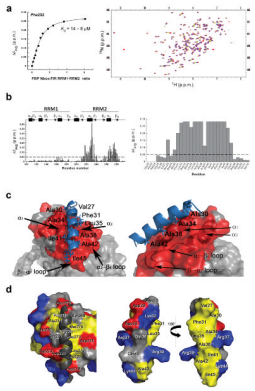

Figure 4.

FBP Nbox interacts with FIR RRM2 using a sparsely packed hydrophobic surface. **(a)** Left – Isotherm for FBP Nbox binding to FIR RRM1-RRM2 (NMR). K_d is reported ± 2 × s.d. Right – Superimposed ^{15}N–^{1}H correlation spectra recorded during a titration of FIR RRM1-RRM2 with FBP Nbox. The spectra are color-coded according to the peptide:protein ratio: from red (0:1) to purple (6:1). **(b)** Left – Weighted chemical shift changes of FIR RRM1-RRM2 upon addition of FBP Nbox *versus* protein sequence. Right – Weighted chemical shift changes of FBP Nbox upon addition of FIR RRM1-RRM2 *versus* peptide sequence. NH peaks that disappear during the titration are assigned a $\Delta\delta_{avg}$ value of 0.28. **(c)** Solution structure of FIR RRM1-RRM2 (surface representation) in complex with FBP Nbox (ribbon representation – blue). FIR RRM1-RRM2 residues showing substantial chemical shift perturbation upon binding to FBP Nbox are colored in red. The hydrophobic residues of FBP Nbox involved in the interaction (left) and the four alanine residues of FBP Nbox in the central part of the interface (right) are labeled. The FIR RRM2 secondary structure elements involved in peptide binding are indicated. This structural representation was generated using the program PYMOL (www.pymol.org). **(d)** Surface representations of FIR RRM2 (left), of the solvent exposed surface of FBP Nbox (middle), and of the FIR-interacting surface of FBP Nbox (right). Hydrophobic residues are shown in yellow, residues with positive and negative charges are shown in blue and red respectively. This structural representation was generated using the program PYMOL (www.pymol.org).

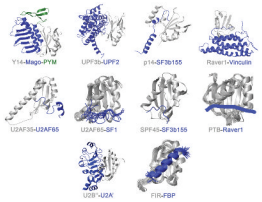

Figure 5.

FIR–FBP interaction represents a novel recognition mode in the RRM family. Ribbon representations of the structures of protein–protein complexes between RRM domains (grey) and their binding partners (blue and green): Y14–Mago–PYM (1rk8), UPF3b–UPF2 (1uw4), p14–SF3b155 (2f9d), Raver1–Vinculin (3h2u), U2AF35–U2AF65 (1jmt), U2AF65–SF1 (1o0p), SPF45–SF3b155 (2peh), U2B″–U2A′ (1a9n) and FIR–FBP (this study). In the PTB–Raver1 complex the Raver1 peptide position is reported (blue) on the structure of PTB RRM2 in the complex with RNA (2adb), according to the published model [22]. U2AF35, U2AF65 and SPF45 RRM domains belong to the UHM subfamily, that bind a conserved Trp residue in the ligand peptides and includes the third RRM of PUF60, an isoform of FIR protein [25]. The cartoon representation of the different structures were generated using the program MOLMOL [26].

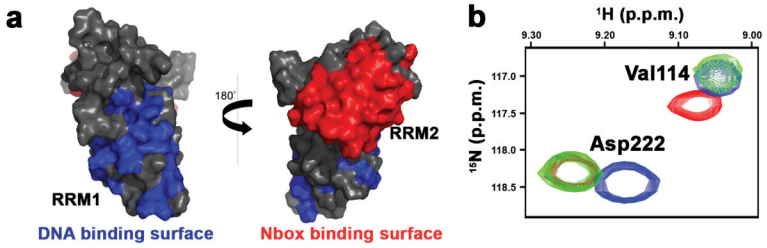

Figure 6.

FIR RRM1-RRM2 independently binds FBP Nbox and ssFUSE on two physically separated sites located on opposite sides of the molecule. **(a)** Surface representation of FIR RRM1-RRM2. Residues showing substantial CSP upon addition of ssFUSE29 or FBP Nbox peptide are colored in blue and red respectively. This structural representation was generated using the program PYMOL (www.pymol.org). **(b)** Superimposed ^{15}N-^{1}H correlation spectra show that FIR RRM1-RRM2 interacts independently with a ssFUSE29 and the FBP Nbox peptide. The spectra of RRM1-RRM2+ssFUSE DNA, RRM1-RRM2+FBP Nbox and RRM1-RRM2 +ssFUSE DNA+FBP Nbox are in blue, red and green respectively. A representative region containing one RRM1 resonance perturbed by DNA binding (Val114) and one RRM2 resonance perturbed by peptide binding (Asp222) is displayed. The chemical shift changes of RRM1-RRM2 peaks in the protein–DNA and protein–peptide complexes are additive in the three molecule complex, indicating independent binding.

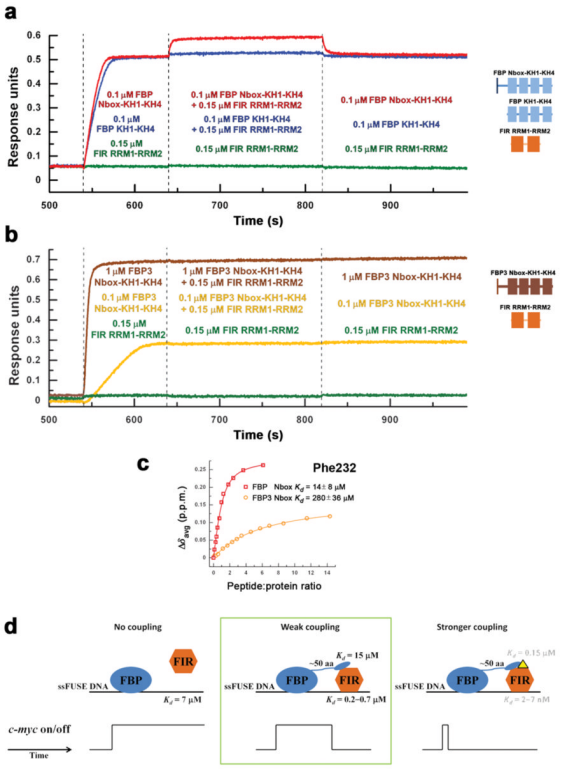

Figure 7.

FBP Nbox recruits FIR to ssFUSE DNA. **(a)** BLI binding assays show that the presence of the Nbox in FBP construct increases the affinity of FIR for the DNA. The BLI biosensors were derivatized with ssFUSE40 and exposed to different combinations of protein constructs (indicated on the right), as reported in the figure. RU changes in three parallel experiments are displayed. **(b)** FBP3 Nbox does not mediate recruitment of FIR to the DNA. BLI biosensors were derivatized with ssFUSE40 and exposed to different combinations of protein constructs (indicated on the right), as reported in the figure. The RU changes observed in three parallel experiments are displayed. **(c)** Isotherms for FBP and FBP3 Nbox binding to FIR RRM1-RRM2 (NMR). K_d are reported ± 2 × s.d. **(d)** Three different modes of FBP–FIR coupling and their effect on FIR binding and *c-myc* transcription. Left – In the absence of a coupling between FBP and FIR the affinity of FIR for the ssFUSE (K_d ~7 μM) would be too low for FIR to bind the ssFUSE. FBP activation of *c-myc* transcription (bottom) would therefore continue unperturbed. Middle – Boxed, the physiological scenario. The weak binding of the Nbox to FIR RRM2 and the 50-amino acid linker between the Nbox and KH1 are responsible for the physiological weak coupling between FBP and FIR. This coupling is necessary to create the required peak in *c-myc* expression (bottom) and regulate the cell cycle. Right – A stronger coupling between FBP and FIR created by, for example, a small molecular weight compound binding at the interface between the two molecules that would increase two orders of magnitude the apparent affinity of FIR for the FBP–ssFUSE complex, would speed FIR recruitment and lead to a shorter peak in *c-myc* expression (bottom).

Table 1

NMR and refinement statistics for protein structures

	FIR RRM1–RRM2 (103–297)	FIR RRM1–RRM2 (103–297) – FBP Nbox (27–52) complex
NMR distance and dihedral constraints		
Distance constraints	4,431	4,647
Total NOE	4,368	4,611
Intra-residue	1,588	1,632
Inter-residue	2,780	2,979
Sequential ($\|i-j\|=1$)	906	878
Medium-range ($\|i-j\|<4$)	487	546
Long-range ($\|i-j\|>5$)	1,387	1,483
Intermolecular	–	72
Hydrogen bonds	63	36
Total dihedral angle restraints	236	280
φ	118	140
ψ	118	140
Structure statistics		
Violations (mean and s.d.)		
Distance constraints (> 0.3 Å) (Å)	0.32 ± 0.02	0.34 ± 0.03
Dihedral angle constraints (> 5°)	– *	6.37 ± 0.98
Max. dihedral angle violation (°)	– *	8.65
Max. distance constraint violation (Å)	0.35	0.42
Deviations from idealized geometry		
Bond lengths (Å)	0.0036 ± 0.0001	0.0036 ± 0.0001
Bond angles (°)	0.480 ± 0.011	0.507 ± 0.008
Impropers (°)	1.46 ± 0.08	1.41 ± 0.06
Average pairwise r.m.s. deviation** (Å)		
Heavy	1.91 ± 0.23	2.03 ± 0.24
Backbone	1.28 ± 0.20	1.40 ± 0.21

* No violations > 5°

** Pairwise r.m.s. deviation was calculated among 20 refined structures (residues 105-288 for FIR RRM1-RRM2 and residues 105-288 and 27-45 for FIR RRM1-RRM2–FBP Nbox complex)